



UNIVERSITY OF LEEDS

This is a repository copy of *Forcing, feedback and internal variability in global temperature trends*.

White Rose Research Online URL for this paper:
<http://eprints.whiterose.ac.uk/83143/>

Version: Accepted Version

Article:

Marotzke, J and Forster, PM (2015) Forcing, feedback and internal variability in global temperature trends. *Nature*, 517 (7536). 565 - 570. ISSN 0028-0836

<https://doi.org/10.1038/nature14117>

Reuse

Unless indicated otherwise, fulltext items are protected by copyright with all rights reserved. The copyright exception in section 29 of the Copyright, Designs and Patents Act 1988 allows the making of a single copy solely for the purpose of non-commercial research or private study within the limits of fair dealing. The publisher or other rights-holder may allow further reproduction and re-use of this version - refer to the White Rose Research Online record for this item. Where records identify the publisher as the copyright holder, users can verify any specific terms of use on the publisher's website.

Takedown

If you consider content in White Rose Research Online to be in breach of UK law, please notify us by emailing eprints@whiterose.ac.uk including the URL of the record and the reason for the withdrawal request.



eprints@whiterose.ac.uk
<https://eprints.whiterose.ac.uk/>

1 **Forcing, feedback, and internal variability in global**
2 **temperature trends**

3

4 Jochem Marotzke, Max Planck Institute for Meteorology, Bundesstrasse 53, 20146

5 Hamburg, Germany; jochem.marotzke@mpimet.mpg.de; phone: +49-40-41173-440;

6 fax: +49-40-41173-366 (corresponding author)

7 Piers M. Forster, School of Earth and Environment, University of Leeds;

8 p.m.forster@leeds.ac.uk

9

10 **Summary**

11 Most current-generation climate models simulate an increase in global mean surface
12 temperature (GMST) since 1998 while observations suggest a warming hiatus. It is still
13 unclear to what extent this mismatch is caused by incorrect model forcing, by incorrect
14 model response to forcing, or by random factors. To place the hiatus in context, we
15 analyse simulations and observations of GMST from 1900 to 2012 and show that the
16 distribution of simulated 15-year trends shows no systematic bias against the
17 observations. Using a multiple regression approach that is physically motivated by
18 surface energy balance, we isolate the impact of radiative forcing, climate feedback, and
19 ocean heat uptake on GMST – with the residual interpreted as internal variability – and
20 assess all possible 15- and 62-year trends. The differences between simulated and
21 observed trends are dominated by (1) random internal variability at 15 years and (2)
22 variations in the radiative forcings used to drive models at 62 years. For either trend
23 length, spread in simulated climate feedback leaves no traceable imprint on GMST
24 trends and thus on the difference between simulations and observations. The claim that
25 climate models systematically overestimate the response to radiative forcing from
26 increasing greenhouse-gas concentrations therefore appears to be unfounded.

27

28

29

30

31 **Introduction**

32

33 The global-mean surface temperature (GMST) has risen in the past fifteen years at a rate
34 that is only one-third to one-half of the average over the second half of the 20th century
35 (e.g., refs. 1-5). This hiatus is not reproduced in most simulations with current-
36 generation climate models, which instead over the period 1998 to 2012 show a larger
37 GMST trend than observed⁵⁻¹⁴. The difference between GMST observations and
38 simulations is caused in part by quasi-random internal climate variability^{5-10,13,14}, which
39 arises because of chaotic processes in the climate system. But part of the difference is
40 likely caused by errors in the model radiative forcing^{5,12,14-16} or in the model response to
41 radiative forcing^{5,14,17,18}. The relative magnitudes of these three contributions are poorly
42 known. Here we quantify how forcing, feedback, and internal climate variability
43 contribute to spread in simulated historical GMST trends and hence to the differences
44 between models and observations.

45

46 We use a three-pronged approach. First, we note that due to quasi-random
47 internal climate variability, the difference between observed and simulated trends
48 likewise contains quasi-random contributions. To avoid focusing too strongly on the
49 particular period 1998 to 2012 – which contains some climate extremes relevant for
50 GMST¹⁹⁻²¹ and is hence unlikely to be reproduced in a simulation containing quasi-
51 random contributions – we analyse GMST trends of a certain length for the entire
52 period 1900 to 2012 (see ref. 13). Second, we quantify the contributions of forcing,
53 climate feedback, ocean heat uptake, and internal variability to simulated GMST trends,
54 through a multiple linear regression approach that is physically motivated by the global
55 surface energy balance. And third, we investigate trends over both 15 and 62 years,

56 representing decadal and multi-decadal timescales, respectively. We combine these
57 three aspects into a new unified conceptual framework, which allows us to put the
58 GMST trends over the 15-year period 1998 to 2012 into appropriate context.

59

60 We first create linear trends from an ordinary-least-squares fit and perform all
61 statistical analyses on these trends. This procedure implies that the analysis must be
62 repeated for each trend length, in contrast to previous work aiming at attributing
63 elements in the observed GMST time series itself. Such elements include effects of
64 volcanic eruptions, solar variability, anthropogenic forcing, El Niño events, and
65 atmospheric dynamic variability including land-sea contrasts^{13,14,22-25}. Because the
66 amplitude of internal variability decreases with increasing trend length^{3,26}, we expect a
67 cleaner breakdown into the individual contributions from forcing, feedback, and internal
68 variability if we focus on one trend length at a time. We analyse trends over 15 and 62
69 years, because these were the trend lengths primarily considered in the
70 Intergovernmental Panel on Climate Change Assessment Report 5 (IPCC AR5, ref. 5).

71

72 **Observed and simulated 15-year trends**

73

74 To gauge whether the difference between simulations and observations is unusual over
75 the hiatus period, we first compare observed and simulated 15-year trends over the
76 entire period from 1900 to 2012 (Fig. 1, see also ref. 13). We use the HadCRUT4
77 observational data set²⁷ and the “historical” simulations conducted under the auspices of
78 the Coupled Model Intercomparison Project Phase 5 (CMIP5, ref. 28), extended for the
79 years 2006 to 2012 with the RCP4.5 scenario runs (Extended Data Fig. 1, Extended

80 Data Table 1). The simulation output is subsampled using the HadCRUT4 data mask¹¹,
81 to account for the effects of incomplete observational coverage^{29,30}.

82

83 Figure 1a contains the joint relative frequency distribution of 15-year GMST
84 trends across the 114 available CMIP5 simulations, as a function of start years since
85 1900 and trend size. Compared to the CMIP5 ensemble, observed trends are distributed
86 in no discernibly preferred way and occur sometimes at the upper end of the ensemble
87 (e.g., start year 1927, best-estimate observed trend larger than 110 of the 114 simulated
88 trends, Fig. 1b) and sometimes at the lower end of the ensemble (e.g., start year 1998,
89 best-estimate observed trend smaller than all 114 simulated trends, Fig. 1c)^{5,13,26}.

90

91 In both cases depicted in Figs. 1b or 1c, fewer than 5% of the simulations lie in
92 one of the tails relative to the observed trend. Hence, if a 5% criterion for statistical
93 significance is used, one would diagnose formal model–observation inconsistency for
94 15-year trends with start years in 1927 and 1998 (ref. 11). But when the comparison is
95 repeated for all start years, the rank that the observed trend would have as a member of
96 the ensemble of simulated trends³¹ shows no apparent bias (Fig. 1e), indicating that the
97 observed and simulated distributions of 15-year trends are broadly consistent with each
98 other. Any position of the observed trend within the ensemble of simulated trends –
99 including a position at or near the margin – is thus dominated by quasi-random effects
100 (although for any particular start year, a non-negligible contribution from systematic
101 errors cannot be excluded).

102

103 The marginal distribution of simulated GMST trends as a function of trend size
104 is wider than the observed distribution of trends (Fig. 1d), a finding consistent with that

105 from the previous generation of climate models³². The width is exaggerated owing to
106 contributions arising at three distinct periods. Some simulated trends with start years
107 from around 1950 to 1960 are more strongly negative than any observed trends since
108 1900, and some simulated trends with start years from around 1960 to 1970 and from
109 around 1985 to 1998 are more strongly positive than any observed trends since 1900
110 (Fig. 1a). All three periods (1950 to 1960, 1960 to 1970, 1985 to 1998) are influenced
111 by volcanic eruptions (Agung in 1963 and Pinatubo in 1991). We speculate that some,
112 though not all, models overestimate the cooling induced by an eruption and the
113 subsequent warming recovery (see, e.g., ref. 12 concerning a confounding role of El
114 Niño).

115
116 The mean over all simulated 15-year trends during the period 1900 to 2012 is at
117 (0.086 ± 0.001) °C per decade (mean \pm s.e.m.; n=11,186) in excellent agreement with the
118 observed (0.088 ± 0.01) °C per decade (mean \pm s.e.m.; n=99). Furthermore, of all 11,186
119 pairwise comparisons that are possible between simulated and observed trends, the
120 observed trend is higher in 53.6% of all cases, slightly above the break-even point.
121 Figure 1 demonstrates that when viewed over the entire period 1900 to 2012, the 15-
122 year GMST trends simulated by the CMIP5 ensemble show no systematic deviation
123 from the observations.

124
125 Our interpretation of Fig. 1 tacitly assumes that simulated multi-model-ensemble
126 spread accurately characterises internal variability, an assumption shared with other
127 interpretations of the position of observed relative to simulated trends (e.g., the
128 reduction in Arctic summer sea ice^{5,33,34}). We now test the validity of this assumption,
129 by identifying deterministic and quasi-random causes of ensemble spread. We exploit

130 the availability of a large number of simulations – 114 realisations with 36 different
131 models, with forcing information available for 75 realisations with 18 different models³⁵
132 (Extended Data Figs. 1 and 2 and Extended Data Table 1) – and investigate the
133 contributions of radiative forcing, climate feedback, and ocean heat uptake to all
134 simulated 15-year and 62-year GMST trends during the period 1900 to 2012.
135

136 **Energy balance and multiple regression**

137
138 Our starting point is the globally averaged energy balance for the surface layer³⁵⁻³⁷. An
139 increasing trend ΔF in effective radiative forcing (ERF) causes an increasing trend ΔT
140 in GMST. This in turn leads to increased outgoing radiation, which in linearised form is
141 written as $\alpha\Delta T$, where α is the climate feedback parameter. Furthermore, the GMST
142 increase leads to increased heat transfer from the surface layer to the subsurface ocean,
143 written again in linearised form as $\kappa\Delta T$, where κ is the ocean heat uptake efficiency.
144 The thermal adjustment of the surface layer to ΔF is expected to occur within a few
145 years³⁵⁻³⁷. This means that for timescales of one to several decades, the surface energy
146 balance is in quasi-steady state and reads

$$147 \quad (\alpha + \kappa)\Delta T = \Delta F , \quad (1)$$

148 which produces the energy-balance “prediction” for the GMST trend

$$149 \quad \Delta T = \Delta F / (\alpha + \kappa). \quad (2)$$

150
151 Each CMIP5 model simulates its own ERF time series over the historical period.
152 These time series were diagnosed previously³⁵; if multiple realisations were available
153 for a model, the ensemble average of the individual diagnosed ERF time series for this

154 model was given³⁵ and is used here. The individual α and κ were previously determined
 155 for each CMIP5 model from a regression of global top-of-atmosphere energy imbalance
 156 against GMST^{5,35,38-41}, in turn based on simulations in which the CO₂ concentration was
 157 quadrupled abruptly. The ranges of α and κ are (0.6–1.8) and (0.45–1.52) Wm⁻²(°C)⁻¹,
 158 respectively. That α and κ in the CMIP5 models might vary with time and climate
 159 state^{42,43} is ignored here. There is some positive though not statistically significant
 160 correlation between α and κ (across the 75-member sub-ensemble, correlation is 0.17, p
 161 = 0.14).

162

163 Each model's α is related to its equilibrium climate sensitivity ECS by

$$164 \quad \text{ECS} = F_{2x} / \alpha, \quad (3)$$

165 where F_{2x} is the effective radiative forcing from a doubling of the pre-industrial
 166 atmospheric CO₂ concentration. The reference value for F_{2x} is 3.7 Wm⁻² (e.g., ref. 44),
 167 but F_{2x} varies between 2.6 Wm⁻² and 4.3 Wm⁻² across the CMIP5 ensemble^{5,38}. In order
 168 not to confound model-response uncertainty with uncertainty from CO₂ forcing, we use
 169 α and not ECS to characterise model response.

170

171 Based on the physical foundation of energy balance (2), we determine the extent
 172 to which the across-ensemble variations of ΔF , α , and κ contribute to the ensemble
 173 spread of GMST trends ΔT , using the 75-member sub-ensemble of CMIP5 historical
 174 simulations for which radiative-forcing information can be obtained from the CMIP5
 175 archive³⁵ (see Extended Data Table 1). The presence of internal variability is included in
 176 our framework by adding a random term to (2), so that our equation is

$$177 \quad \Delta T = \Delta F / (\alpha + \kappa) + \varepsilon. \quad (4)$$

178 Because (4) assumes an increasing trend in ERF, its validity is somewhat questionable
 179 following a volcanic eruption (e.g., ref. 25). On the other hand, Extended Data Figure 3
 180 shows that overall we see a reliable relationship between ERF and GMST trends in the
 181 CMIP5 ensemble, even if the ERF trend is negative.

182

183 We make the connection to multiple linear regression by writing each quantity
 184 as

$$185 \quad x = \bar{x} + x', \quad (5)$$

186 where the overbar marks the ensemble average and the prime the across-ensemble
 187 variation. Linear expansion of (4) thus produces

$$188 \quad \Delta\bar{T} + \Delta T' = \frac{\Delta\bar{F}}{\bar{\alpha} + \bar{\kappa}} + \frac{1}{\bar{\alpha} + \bar{\kappa}} \Delta F' - \frac{\Delta\bar{F}}{(\bar{\alpha} + \bar{\kappa})^2} \alpha' - \frac{\Delta\bar{F}}{(\bar{\alpha} + \bar{\kappa})^2} \kappa' + \varepsilon. \quad (6)$$

189 This equation holds for each start year separately and suggests the regression model

$$190 \quad \Delta T'_j = \beta_0 + \beta_1 \Delta F'_j + \beta_2 \alpha'_j + \beta_3 \kappa'_j + \varepsilon_j; \quad j = 1, \dots, 75. \quad (7)$$

191 We thus perform for each start year a multiple linear regression of $\Delta T'$ against $\Delta F'$, α' ,
 192 and κ' . The regression residual ε is interpreted as the contribution from internal
 193 variability. The complete regression-based prediction for GMST trend is obtained by
 194 adding the ensemble-mean trend to the regression for the across-ensemble variations:

$$195 \quad \Delta\hat{T}_{\text{reg},j} = \Delta\bar{T} + \hat{\beta}_0 + \hat{\beta}_1 \Delta F'_j + \hat{\beta}_2 \alpha'_j + \hat{\beta}_3 \kappa'_j; \quad j = 1, \dots, 75, \quad (8)$$

196 where the caret marks the regression estimate. Note that for a model that has multiple
 197 realisations, the same $\Delta F'_j$, α'_j or κ'_j is counted multiple times. The regression is
 198 performed separately for each period length over which trends are computed. We will
 199 interpret the ensemble spread of the regression result $\Delta\hat{T}_{\text{reg},j}$, $j = 1, \dots, 75$, as the

200 deterministic spread and the spread $\hat{\varepsilon}_j$, $j = 1, \dots, 75$, of the residuals as the quasi-random
201 spread.

202

203 **Deterministic vs. quasi-random spread**

204

205 For 15-year GMST trends, deterministic across-ensemble variations are smaller than
206 internal variability, as shown by the comparison of the regression-based ensemble
207 spread with the regression residuals (Figs. 2b and c, respectively). The regression result
208 shows substantial time-dependence in ensemble spread only for 15-year periods
209 influenced by major volcanic eruptions, in particular the Agung eruption in 1963 (Fig.
210 2b; the deterministic ensemble spread is particularly large in these periods, see
211 Extended Data Fig. 4a). The distribution of residuals shows little time-dependence, as
212 witnessed by spread that is similar for all start years (Figs. 2c–f). The generally weak
213 time-dependence of the spread suggests that we can estimate the magnitudes of
214 deterministic spread and internal variability from the marginal distributions obtained by
215 time-averaging the distributions shown in Figs. 2b and 2c, respectively. The 5–95%
216 range is 0.11 °C per decade for the regression result and 0.26 °C per decade for the
217 residuals; internal variability thus dominates deterministic spread by a factor of two-
218 and-a-half. The dominance of internal variability in the ensemble spread of the 15-year
219 GMST trends indicates that, viewed over the entire period 1900 to 2012, no systematic
220 model error needs to be invoked when trying to explain differences between simulated
221 and observed trends. In particular, the GMST spread due to feedback α is not
222 systematically larger than spread from either ERF trend or ocean heat uptake efficiency

223 and is much smaller than internal variability (Extended Data Fig. 4 and Fig. 2; see also
224 ref. 12).

225

226 For any given start year, the residual spread is very similar to the full ensemble
227 spread, implying that we can indeed use the ensemble spread as a measure of internal
228 variability (compare Figs. 1b and c to Figs. 2d and e). Furthermore, identifying the
229 ensemble spread of the regression residuals with internal variability allows us to
230 characterise the component of observational uncertainty that arises from internal
231 variability (Figs. 2a and f). This uncertainty does not concern the construction of the
232 global average from individual station data (which has much smaller uncertainty⁵) but
233 relates to the question of whether an observed trend is statistically significant
234 (detectable) given serial correlation arising from internal variability¹⁸. Our model-based
235 estimate of 0.26 °C per decade for the 5–95% confidence interval for observed 15-year
236 GMST trends is slightly larger than the AR5 serial-correlation-based estimate for the
237 uncertainty of the observed GMST trend over the hiatus period (0.2 °C per decade, see
238 ref. 4). We deem this an acceptable agreement given that the estimates were obtained
239 through completely different approaches. We further note that the CMIP5 ensemble has
240 been assessed to be generally consistent with observed historical decadal variability in
241 GMST⁵, although on average it overestimates somewhat the global variability in the
242 lower troposphere⁴⁵.

243

244 For most of the historical period, the entire ensemble of regression-based
245 simulated 15-year GMST trends lies within the model-estimated 5–95% confidence
246 interval of the observations (Fig. 2a). The regression-based simulated ensemble partially
247 falls outside this interval during the cooling following the Agung eruption and the

248 subsequent warming recovery, as well as for start dates after 1990, which include the
249 warming recovery following the Pinatubo eruption and the surface-warming hiatus (Fig.
250 2a). Because the phases of volcanically driven cooling and subsequent warming
251 coincide with larger regression spread due to ERF trend (Extended Data Fig. 4), we
252 speculate that the implementation of volcanic forcing requires improvement in some
253 climate models.

254

255 The ensemble spread of 62-year GMST trends is dominated by internal
256 variability for start years early in the 20th century, but for start years from 1910 onward,
257 the deterministic spread increases and dominates for start years 1920 and later (Fig. 3).
258 The 5–95% range of the regression residuals is 0.059 °C per decade, compared to a
259 deterministic range of 0.032 °C per decade for start year 1900 and 0.093 °C per decade
260 for start year 1951. The 5–95% deterministic range for all 62-year trends is 0.081 °C per
261 decade, which is larger by one-third than the 5–95% range from internal variability.
262 Nevertheless, we see a substantial influence of internal variability even for GMST
263 trends over 62 years.

264

265 When observational uncertainty is accounted for – based again on the 5–95%
266 confidence interval derived from quasi-random model spread – the ensemble-mean
267 simulated 62-year GMST trend is consistent with the observed trend for all start years
268 after around 1915; before that, the simulations tend to warm too little (Fig. 3a). After
269 around 1945, the ensemble-mean simulated 62-year trend lies above the observed trend,
270 although their difference is smaller than the range of internal variability. From around
271 1925 onward, both the largest and the smallest individual regression-based simulated

272 trends lie outside the range defined by observations plus internal variability and would
273 hence be judged to be inconsistent with observations (Fig. 3a).

274

275 The cause of this inconsistency can be traced almost entirely to the contribution
276 to the regression by the ERF trend (Fig. 3). By contrast, the magnitude of the
277 contributions by α and κ is around 0.01 °C per decade or less for all start years (Figs. 3e
278 and f). The deterministic ensemble spread in 62-year GMST trend is hence dominated
279 by the spread in ERF throughout the 20th century (Fig. 3).

280

281

282 **Discussion**

283

284 Viewed over the entire period since 1900, the differences between simulated and
285 observed 15-year trends in GMST are dominated by internal variability and hence arise
286 largely by coincidence, with a minor contribution from volcanic forcing that is
287 sometimes too strong in some models (Fig. 2). Furthermore, we confirm and extend to
288 all 15-year radiative-forcing trends since 1900, the AR5 assessment for the hiatus
289 period⁵ that the CMIP5 models show little systematic bias when comparing against the
290 AR5 best-estimate radiative-forcing trend⁴⁶ – despite the substantial scatter about the
291 ensemble mean (Extended Data Fig. 2).

292

293 The generally dominant role of internal variability in shaping simulated 15-year
294 GMST trends implies that internal variability also dominates the difference between
295 simulations and observations during the hiatus period. This conclusion sharpens
296 considerably the relative roles of internal variability, forcing error, and response error,

297 compared to the corresponding AR5 assessment⁵. While there is no obvious
298 contribution of forcing bias in the CMIP5 models (Extended Data Fig. 2), the diagnosed
299 radiative forcing is uncertain³⁵. Hence our analysis cannot rule out a small contribution
300 from a systematic forcing bias^{12,15,16,46-48} in the models. In particular, volcanic forcing is
301 estimated to contribute to the difference between simulations and observations by up to
302 15% over 1998 to 2012 in ref. 12, with large uncertainty in the magnitude, a
303 contribution that our method cannot detect. Furthermore, the period 1998 to 2012 stands
304 out as the only one during which the HadCRUT4 15-year GMST trend falls entirely
305 outside the CMIP5 ensemble (if only narrowly), suggesting that the CMIP5 models
306 could be missing a cooling contribution from the radiative forcing during the hiatus
307 period^{12,15,16,46-48}, or that there has been an unusual enhancement of ocean heat uptake
308 not simulated by any model¹⁹.

309

310 For 62-year GMST trends since 1900, the difference between simulations and
311 observations is dominated by the spread in radiative-forcing trend in the models, with a
312 smaller yet substantial influence of internal variability (Fig. 3). Our simple regression-
313 based estimate of internal variability in 62-year GMST trends corresponds to a 17–83%
314 range of ± 0.11 °C for the temperature change over six decades, which is in excellent
315 agreement with the value of ± 0.10 °C that has been found for the period 1951 to 2010
316 using much more sophisticated formal methods of detection and attribution¹⁸.

317

318 There is scientific, political, and public debate regarding the question of whether
319 the GMST difference between simulations and observations during the hiatus period
320 might be a sign of an equilibrium model response to a given radiative forcing that is
321 systematically too strong, or equivalently, of a simulated climate feedback α that is

322 systematically too small (cf., (3)). By contrast, we find no substantive physical or
323 statistical connection between simulated climate feedback and simulated GMST trends
324 over the hiatus or any other period, either for 15- or for 62-year trends (Figs. 2 and 3,
325 Extended Data Fig. 4). The role of simulated climate feedback in explaining the
326 difference between simulations and observations is hence minor or even negligible. By
327 implication, the comparison of simulated and observed GMST trends does not permit
328 inference about which magnitude of simulated climate feedback – ranging from 0.6 to
329 $1.8 \text{ Wm}^{-2}(\text{°C})^{-1}$ in the CMIP5 ensemble – better fits the observations. Because observed
330 GMST trends do not allow us to distinguish between simulated climate feedback that
331 varies by a factor of three, the claim that climate models systematically overestimate the
332 GMST response to radiative forcing from increasing greenhouse-gas concentrations
333 appears to be unfounded.

334

335

336 **References**

- 337 1. Knight, J. et al. Do global temperature trends over the last decade falsify climate
338 predictions? [In: State of the Climate in 2008]. Bull. Am. Met. Soc. **90**, S22-S23
339 (2009).
- 340 2. Wang, S. et al. Does the global warming pause in the last decade: 1999-2008?
341 Adv. Clim. Change Res. **1**, 49-54 (2010).
- 342 3. Liebmann, B., Dole, R. M., Jones, C., Blade, I. & Allured, D. Influence of
343 choice of time period on global surface temperature trend estimates. Bull. Am.
344 Met. Soc. **91**, 1485-1491 (2010).
- 345 4. Hartmann, D. L. et al. in Climate Change 2013: The Physical Science Basis.
346 Contribution of Working Group I to the Fifth Assessment Report of the
347 Intergovernmental Panel on Climate Change (eds T. F. Stocker et al.) 159-254
348 (Cambridge University Press, 2013).
- 349 5. Flato, G. et al. in Climate Change 2013: The Physical Science Basis.
350 Contribution of Working Group I to the Fifth Assessment Report of the
351 Intergovernmental Panel on Climate Change (eds T. F. Stocker et al.) 741-866
352 (Cambridge University Press, 2013).
- 353 6. Meehl, G. A., Arblaster, J. M., Fasullo, J. T., Hu, A. & Trenberth, K. E. Model-
354 based evidence of deep-ocean heat uptake during surface-temperature hiatus
355 periods. Nature Clim. Change **1**, 360-364 (2011).
- 356 7. Meehl, G. A. & Teng, H. Case studies for initialized decadal hindcasts and
357 predictions for the Pacific region. Geophys. Res. Lett. **39**, L22705, doi:
358 22710.21029/22012GL053423 (2012).

- 359 8. Meehl, G. A., Hu, A., Arblaster, J. M., Fasullo, J. & Trenberth, K. E. Externally
360 Forced and Internally Generated Decadal Climate Variability Associated with
361 the Interdecadal Pacific Oscillation. *J. Climate* **26**, 7298-7310 (2013).
- 362 9. Doblas-Reyes, F. J. et al. Initialized near-term regional climate change
363 prediction. *Nature Comm.* **4**, 1715, doi:1710.1038/ncomms2704 (2013).
- 364 10. Guemas, V., Doblas-Reyes, F. J., Andreu-Burillo, I. & Asif, M. Retrospective
365 prediction of the global warming slowdown in the past decade. *Nature Clim.*
366 *Change* **3**, 649-653 (2013).
- 367 11. Fyfe, J. C., Gillett, N. P. & Zwiers, F. W. Overestimated global warming over
368 the past 20 years. *Nature Clim. Change* **3**, 767-769 (2013).
- 369 12. Santer, B. D. et al. Volcanic contribution to decadal changes in tropospheric
370 temperature. *Nature Geosci.* **7**, 185-189 (2014).
- 371 13. Risbey, J. S. et al. Well-estimated global surface warming in climate projections
372 selected for ENSO phase. *Nature Clim. Change* **4**, 835-840 (2014).
- 373 14. Huber, M. & Knutti, R. Natural variability, radiative forcing and climate
374 response in the recent hiatus reconciled. *Nature Geosci.* **7**, 651-656 (2014).
- 375 15. Solomon, S. et al. The persistently variable "background" stratospheric aerosol
376 layer and global climate change. *Science* **333**, 866-870 (2011).
- 377 16. Schmidt, G. A., Shindell, D. T. & Tsigaridis, K. Reconciling warming trends.
378 *Nature Geosci.* **7**, 158-160 (2014).
- 379 17. Stott, P., Good, P., Jones, G., Gillett, N. & Hawkins, E. The upper end of
380 climate model temperature projections is inconsistent with past warming. *Env.*
381 *Res. Let.* **8** (2013).
- 382 18. Bindoff, N. L. et al. in *Climate Change 2013: The Physical Science Basis.*
383 *Contribution of Working Group I to the Fifth Assessment Report of the*

- 384 Intergovernmental Panel on Climate Change (eds T. F. Stocker et al.) 867-952
385 (Cambridge University Press, 2013).
- 386 19. England, M. H. et al. Recent intensification of wind-driven circulation in the
387 Pacific and the ongoing warming hiatus. *Nature Clim. Change* **4**, 222-227
388 (2014).
- 389 20. Cohen, J. L., Furtado, J. C., Barlow, M., Alexeev, V. A. & Cherry, J. E.
390 Asymmetric seasonal temperature trends. *Geophys. Res. Lett.* **39**, L04705,
391 doi:04710.01029/02011GL050582 (2012).
- 392 21. Kosaka, Y. & Xie, S.-P. Recent global-warming hiatus tied to equatorial Pacific
393 surface cooling. *Nature* **501**, 403-407 (2013).
- 394 22. Lean, J. L. & Rind, D. H. How will Earth's surface temperature change in future
395 decades? *Geophys. Res. Lett.* **36** (2009).
- 396 23. Foster, G. & Rahmstorf, S. Global temperature evolution 1979-2010. *Env. Res.*
397 *Let.* **6** (2011).
- 398 24. Kaufmann, R. K., Kauppi, H., Mann, M. L. & Stock, J. H. Reconciling
399 anthropogenic climate change with observed temperature 1998-2008. *Proc. Natl.*
400 *Acad. Sci. U. S. A.* **108**, 11790-11793 (2011).
- 401 25. Thompson, D. W. J., Wallace, J. M., Jones, P. D. & Kennedy, J. J. Identifying
402 signatures of natural climate variability in time series of global-mean surface
403 temperature: Methodology and insights. *J. Climate* **22**, 6120-6141 (2009).
- 404 26. Santer, B. D. et al. Separating signal and noise in atmospheric temperature
405 changes: The importance of timescale. *J. Geophys. Res.-Atmos.* **116**, D22105
406 (2011).
- 407 27. Morice, C. P., Kennedy, J. J., Rayner, N. A. & Jones, P. D. Quantifying
408 uncertainties in global and regional temperature change using an ensemble of

- 409 observational estimates: The HadCRUT4 data set. *J. Geophys. Res.-Atmos.* **117**
410 (2012).
- 411 28. Taylor, K. E., Stouffer, R. J. & Meehl, G. A. An Overview of CMIP5 and the
412 Experiment Design. *Bull. Am. Met. Soc.* **93**, 485-498 (2012).
- 413 29. Cowtan, K. & Way, R. G. Coverage bias in the HadCRUT4 temperature series
414 and its impact on recent temperature trends. *Quart. J. Roy. Met. Soc.* **140**, 1935-
415 1944 (2014).
- 416 30. Simmons, A. J., Willett, K. M., Jones, P. D., Thorne, P. W. & Dee, D. P. Low-
417 frequency variations in surface atmospheric humidity, temperature, and
418 precipitation: Inferences from reanalyses and monthly gridded observational
419 data sets. *J. Geophys. Res.-Atmos.* **115**, D01110 (2010).
- 420 31. Anderson, J. L. A method for producing and evaluating probabilistic forecasts
421 from ensemble model integrations. *J. Climate* **9**, 1518-1530 (1996).
- 422 32. Easterling, D. R. & Wehner, M. F. Is the climate warming or cooling? *Geophys.*
423 *Res. Lett.* **36**, L08706, doi: 08710.01029/02009GL037810 (2009).
- 424 33. Stroeve, J. C. et al. Trends in Arctic sea ice extent from CMIP5, CMIP3 and
425 observations. *Geophys. Res. Lett.* **39** (2012).
- 426 34. Notz, D., Haumann, F. A., Haak, H., Jungclaus, J. H. & Marotzke, J. Arctic sea-
427 ice evolution as modeled by Max Planck Institute for Meteorology's Earth
428 system model. *J. Adv. Model. Earth Sys.* **5**, 173-194 (2013).
- 429 35. Forster, P. M. et al. Evaluating adjusted forcing and model spread for historical
430 and future scenarios in the CMIP5 generation of climate models. *J. Geophys.*
431 *Res.-Atmos.* **118**, 1-12, doi: 10.1002/jgrd.50174 (2013).

- 432 36. Gregory, J. M. & Forster, P. M. Transient climate response estimated from
433 radiative forcing and observed temperature change. *J. Geophys. Res.-Atmos.* **113**
434 (2008).
- 435 37. Held, I. M. et al. Probing the fast and slow components of global warming by
436 returning abruptly to preindustrial forcing. *J. Climate* **23**, 2418-2427 (2010).
- 437 38. Andrews, T., Gregory, J. M., Webb, M. J. & Taylor, K. E. Forcing, feedbacks
438 and climate sensitivity in CMIP5 coupled atmosphere-ocean climate models.
439 *Geophys. Res. Lett.* **39**, L09712, doi: 09710.01029/02012GL051607 (2012).
- 440 39. Kuhlbrodt, T. & Gregory, J. M. Ocean heat uptake and its consequences for the
441 magnitude of sea level rise and climate change. *Geophys. Res. Lett.* **39** (2012).
- 442 40. Vial, J., Dufresne, J.-L. & Bony, S. On the interpretation of inter-model spread
443 in CMIP5 climate sensitivity estimates. *Clim. Dyn.*, 1-24 (2013).
- 444 41. Gregory, J. M. et al. A new method for diagnosing radiative forcing and climate
445 sensitivity. *Geophys. Res. Lett.* **31** (2004).
- 446 42. Block, K. & Mauritsen, T. Forcing and feedback in the MPI-ESM-LR coupled
447 model under abruptly quadrupled CO₂. *J. Adv. Model. Earth Sys.* **5**, 676-691
448 (2013).
- 449 43. Meraner, K., Mauritsen, T. & Voigt, A. Robust increase in equilibrium climate
450 sensitivity under global warming. *Geophys. Res. Lett.* **40**, 5944-5948 (2013).
- 451 44. Forster, P. et al. in *Climate Change 2007: The Physical Science Basis.*
452 *Contribution of Working Group I to the Fourth Assessment Report of the*
453 *Intergovernmental Panel on Climate Change* (eds S. Solomon et al.) 129-234
454 (Cambridge University Press,, 2007).
- 455 45. Santer, B. D. et al. Identifying human influences on atmospheric temperature.
456 *Proc. Natl. Acad. Sci. U. S. A.* **110**, 26-33 (2013).

- 457 46. Myhre, G. et al. in *Climate Change 2013: The Physical Science Basis*.
458 *Contribution of Working Group I to the Fifth Assessment Report of the*
459 *Intergovernmental Panel on Climate Change* (eds T. F. Stocker et al.) 659-740
460 (Cambridge University Press, , 2013).
- 461 47. Fyfe, J. C., von Salzen, K., Cole, J. N. S., Gillett, N. P. & Vernier, J. P. Surface
462 response to stratospheric aerosol changes in a coupled atmosphere-ocean model.
463 *Geophys. Res. Lett.*, DOI: 10.1002/grl.50156 (2013).
- 464 48. Ridley, D. A. et al. Total volcanic stratospheric aerosol optical depths and
465 implications for global climate change. *Geophys. Res. Lett.*, in press, doi:
466 10.1002/2014GL061541 (2014).
- 467
- 468

469 **Acknowledgements**

470 We are indebted to John Fyfe for making his CMIP5 GMST dataset available to us, and
471 to Dirk Notz, Ben Santer, and an anonymous reviewer for helpful comments on the
472 manuscript. We acknowledge the World Climate Research Programme's Working
473 Group on Coupled Modelling, which is responsible for CMIP, and we thank the climate
474 modelling groups (names of models listed in Extended Data Table 1) for producing and
475 making available their model output. For CMIP the U.S. Department of Energy's
476 Program for Climate Model Diagnosis and Intercomparison provides coordinating
477 support and led development of software infrastructure in partnership with the Global
478 Organization for Earth System Science Portals. This work was supported by the Max
479 Planck Society for the Advancement of Science (JM) and by a Royal Society Wolfson
480 Merit Award and EPSRC grant EP/1014721/1 (PMF).

481

482 **Author contributions**

483 Both authors jointly designed the study. JM analysed the data and wrote the manuscript.
484 Both authors discussed the results and the manuscript.

485

486 **Author information**

487 Correspondence and requests for materials should be addressed to
488 jochem.marotzke@mpimet.mpg.de. The authors declare no competing financial
489 interests. Reprints and permissions information is available at www.nature.com/reprints.

490

491

492 **Figure legends**

493

494 **Figure 1.** Simulated and observed 15-year GMST trends since 1900. (a) Joint relative
495 frequency distribution of GMST trends as a function of start year and trend size, based
496 on the full 114-member ensemble (in bins of 0.025 °C per decade; coloured shading).
497 Circles mark the observed trend from the HadCRUT4 data set²⁷. (b) Vertical cross-
498 section of (a) for start year 1927; vertical line marks the observed trend. (c) As (b) but
499 for start year 1998. (d) Marginal distribution of simulated GMST trend as a function of
500 trend size (coloured shading), obtained by time-averaging the joint distribution in (a);
501 observed trend distribution (grey shading). (e) Frequency distribution of the rank that
502 the observed trend would have as a member of the model ensemble (rank 1: observed
503 trend smaller than all simulations; rank 115: observed trend larger than all simulations);
504 bin size is five. All histograms are normalised such that their area integral is unity. In
505 (a), each vertical cross section is normalised.

506

507 **Figure 2.** Regression-based and observed 15-year GMST trends since 1900. (a)
508 Shading: Joint relative frequency distribution of regression-based GMST trends (from
509 equation (8)) as a function of start year and trend size (in bins of 0.025 °C per decade),
510 based on the reduced 75-member ensemble for which forcing information is available.
511 Thick red line marks the ensemble average; thick black line the observed trend;
512 whiskers the 5–95% confidence range derived from (f). (b) Joint relative frequency
513 distribution of regression result (from equation (8) but without the ensemble-mean
514 trend) as a function of start year and trend size (in bins of 0.025 °C per decade). The p-
515 value of the regression has a median across start years of 0.075, based on the null
516 hypothesis that all regression coefficients are zero. (c) Joint relative frequency

517 distribution of regression residual as a function of start year and trend size (in bins of
518 0.025 °C per decade). (d) Vertical cross-section of (c) for start year 1927. (e) Vertical
519 cross-section of (c) for start year 1998. (f) Marginal distribution of regression residual
520 as a function of trend size, obtained by time-averaging the joint distribution in (c). All
521 histograms are normalised such that their area integral is unity. In (a)–(c), each vertical
522 cross section is normalised. All ordinate ranges are identical.

523

524 **Figure 3.** Regression-based and observed 62-year GMST trends since 1900. (a)
525 Shading: Joint relative frequency distribution of regression-based GMST trends (from
526 equation (8)) as a function of start year and trend size, based on the reduced 75-member
527 ensemble for which forcing information is available. Thick red line marks the ensemble
528 average; thick black line the observed trend; whiskers the 5–95% confidence range
529 derived from the marginal distribution of (c). (b) Joint relative frequency distribution of
530 regression result (from equation (8) but without the ensemble-mean trend) as a function
531 of start year and trend size. All p-values of the regression are below 0.001, based on the
532 null hypothesis that all regression coefficients are zero. (c) Joint relative frequency
533 distribution of regression residual as a function of start year and trend size. (d) Joint
534 relative frequency distribution of regression contribution from trend in effective
535 radiative forcing. (e) Joint relative frequency distribution of regression contribution
536 from climate feedback parameter α . (f) Joint relative frequency distribution of
537 regression contribution from ocean heat uptake efficiency κ . In all joint relative
538 frequency distributions, GMST trend is collected in bins of 0.0125 °C per decade, and
539 each vertical cross section is normalised such that its area integral is unity. All ordinate
540 ranges are identical.

541 **Extended Data figure and table legends**

542

543 **Extended Data Figure 1.** Observed and simulated time series of the anomalies in
544 annually averaged global-mean surface temperature (GMST), from 1900 to 2012. All
545 anomalies are differences from the 1961–1990 time-mean of each individual time series.
546 GMST is the globally averaged merged surface temperature (2 m height over land and
547 surface temperature over the ocean). The figure shows single simulations for the CMIP5
548 models (thin lines), the multi-model ensemble mean (thick red line), and the
549 HadCRUT4²⁷ observations (thick black line). All model results have been sub-sampled
550 using the HadCRUT4 observational data mask¹¹. (a) 114 realisations from the CMIP5
551 archive, obtained with 36 different models. (b) Subset of 75 realisations with the 18
552 different models for which information on effective radiative forcing (ERF) is
553 available³⁵ (see Extended Data Table 1). The two model ensembles are nearly
554 indistinguishable.

555

556 **Extended Data Figure 2.** Time series of trends in effective radiative forcing (ERF), as
557 a function of start year. (a) 15-year trends; (b) 62-year trends. Thin coloured lines:
558 individual models as diagnosed previously³⁵; if multiple realisations were available for a
559 model, the ensemble average of the individual diagnosed ERF time series for this model
560 was given³⁵ and is shown here. Thick red line: ensemble average over all models. Thick
561 black line: best estimate from IPCC AR5 (ref. 46), including for illustration the 5–95%
562 uncertainty range for the periods 1984–1998 (a) and 1951–2011 (b), taken from Fig.
563 8.19 in ref. 46. These uncertainty ranges, both of which are around 0.2 Wm^{-2} per
564 decade, do not take into account observational biases such as diagnosed in ref. 48.
565 Despite the scatter of the CMIP5 ensemble trends, the ensemble mean is in good

566 agreement with the AR5 best estimate for almost all start years. The IPCC AR5 best-
567 estimate ERF sums time series of forcing across individual forcing terms. Individual
568 time series of AR5 ERF were derived in different ways. Greenhouse-gas concentrations
569 (observed or inferred), stratospheric aerosol optical depth, and total solar irradiance
570 were used to derive estimates of radiative forcing using simple formulae. Surface albedo
571 forcing was derived from estimated anthropogenic vegetation trends. Ozone and aerosol
572 forcings were derived from chemical transport model results with aspects of the forcing
573 constrained by other modelling approaches or observations, or both. ERF sums rapid
574 adjustments with traditional radiative forcings (RFs). Most time series in AR5 were
575 based on traditional radiative forcings, and only CO₂ and aerosol forcings included an
576 assessment of the rapid adjustment. In other cases ERF and RFs were assumed to be the
577 same. The AR5 ERF for the most recent 2000–2011 period included updated estimates
578 of volcanic and solar forcing, taking into account the broader 2008/9 solar minimum
579 and post-2000 volcanic activity⁴⁶. These two cooling influences are not included in the
580 CMIP5 ERF; it is hence surprising and unexplained why the CMIP5 ensemble-mean of
581 15-year ERF trends lies below the best-estimate AR5 ERF trend for the latest start years
582 in (a).

583

584 **Extended Data Figure 3.** Joint relative frequency distribution as a function of GMST
585 trend and ERF trend, for the reduced 75-member ensemble for which forcing
586 information is available and all start years. (a) 15-year trends; bin sizes are 0.025 °C per
587 decade and 0.05 Wm⁻² per decade for GMST and ERF trend, respectively. (b) 62-year
588 trends; bin sizes are 0.0125 °C per decade and 0.025 Wm⁻² per decade for GMST and
589 ERF trend, respectively. The “climate resistance”, ρ , is given by $\rho = \alpha + \kappa$ (refs. 35-37).

590 Each joint distribution is normalised such that its area integral is unity. Notice the
591 different axes, reflecting the much tighter correlation of the 62-year trends.

592

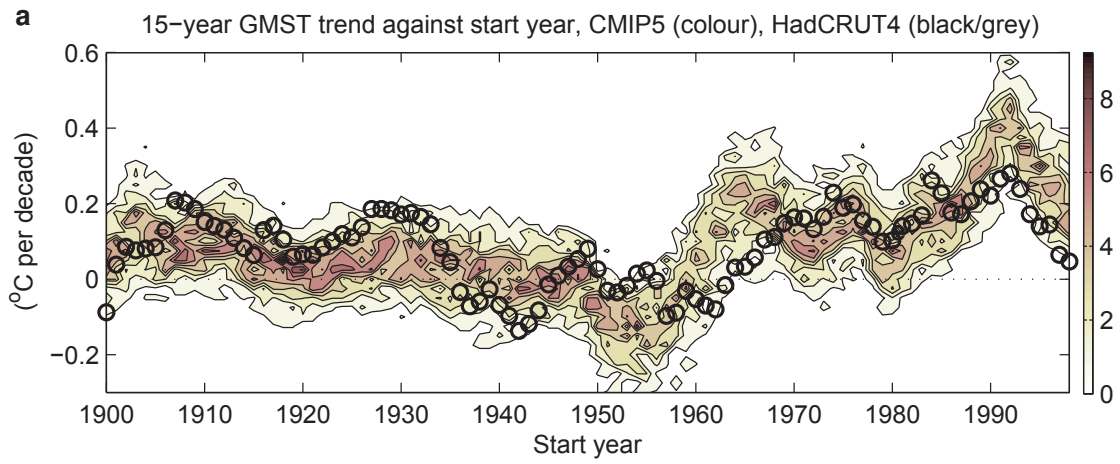
593

594 **Extended Data Figure 4.** Regression-based 15-year GMST trends since 1900. (a) Joint
595 relative frequency distribution of regression result (from equation (8) but without the
596 ensemble-mean trend) as a function of start year and trend size. The p-values of the
597 regression have a median across start years of 0.075, based on the null hypothesis that
598 all regression coefficients are zero. (b) Joint relative frequency distribution of regression
599 contribution from trend in effective radiative forcing (ERF). (c) Joint relative frequency
600 distribution of regression contribution from climate feedback parameter α . (d) Joint
601 relative frequency distribution of regression contribution from ocean heat uptake
602 efficiency κ . In all joint relative frequency distributions, GMST trend is collected in
603 bins of 0.025 °C per decade, and each vertical cross section is normalised such that its
604 area integral is unity.

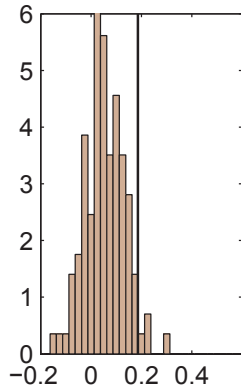
605

606 **Extended Data Table 1.** CMIP5 models used in this study. The originating institutions
607 and publications documenting the models are listed comprehensively in Table 9.A1 of
608 ref. 5.

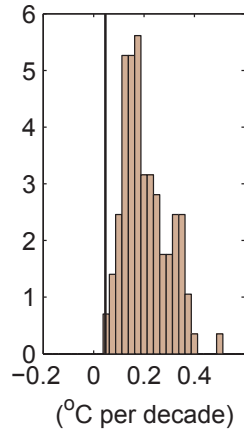
609



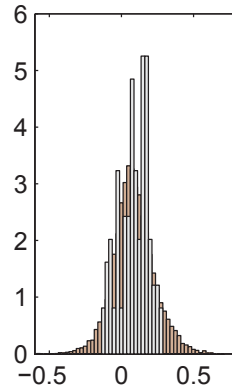
b 1927–1941



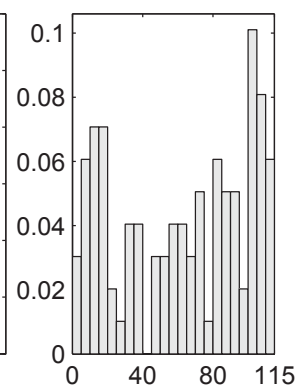
c 1998–2012



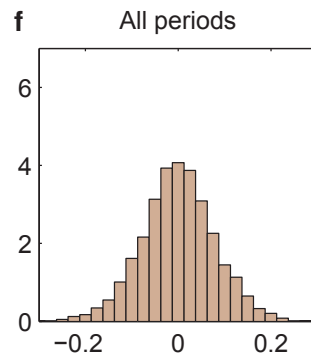
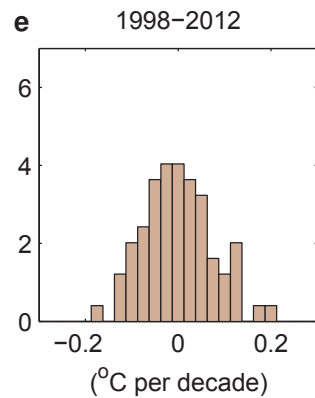
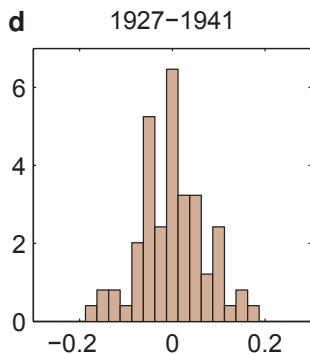
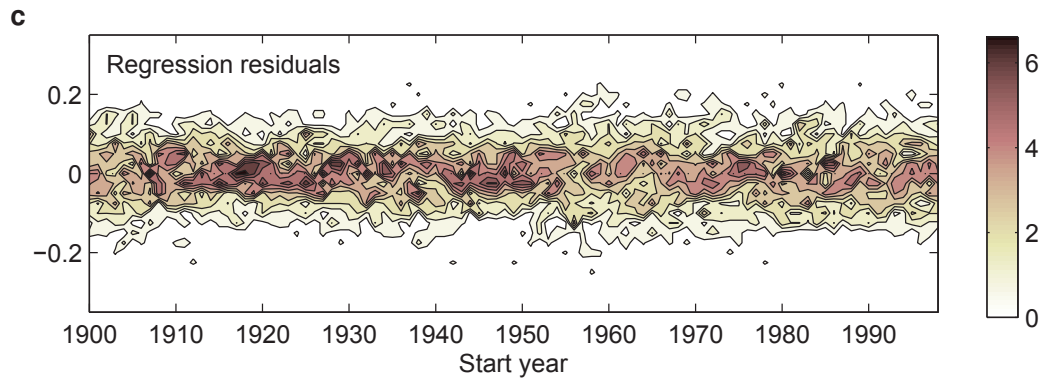
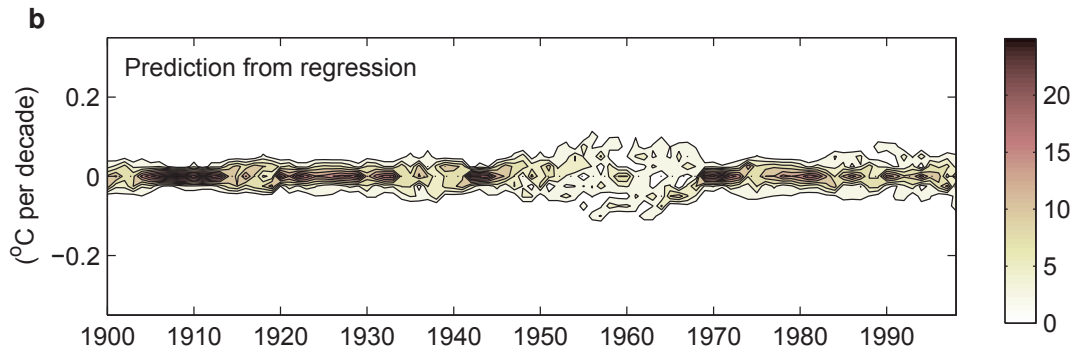
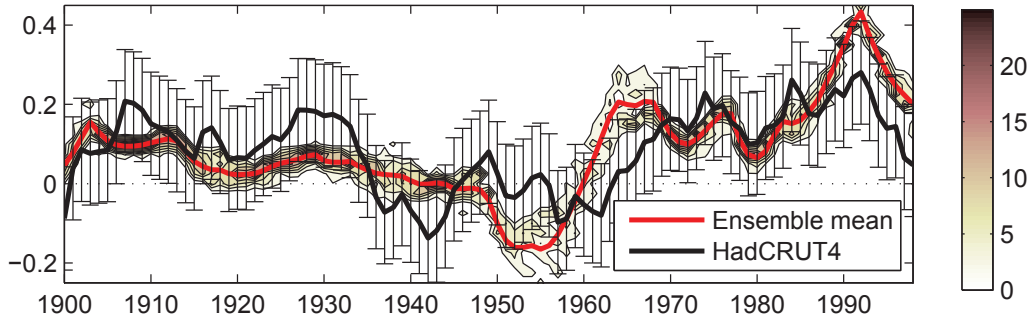
d All periods

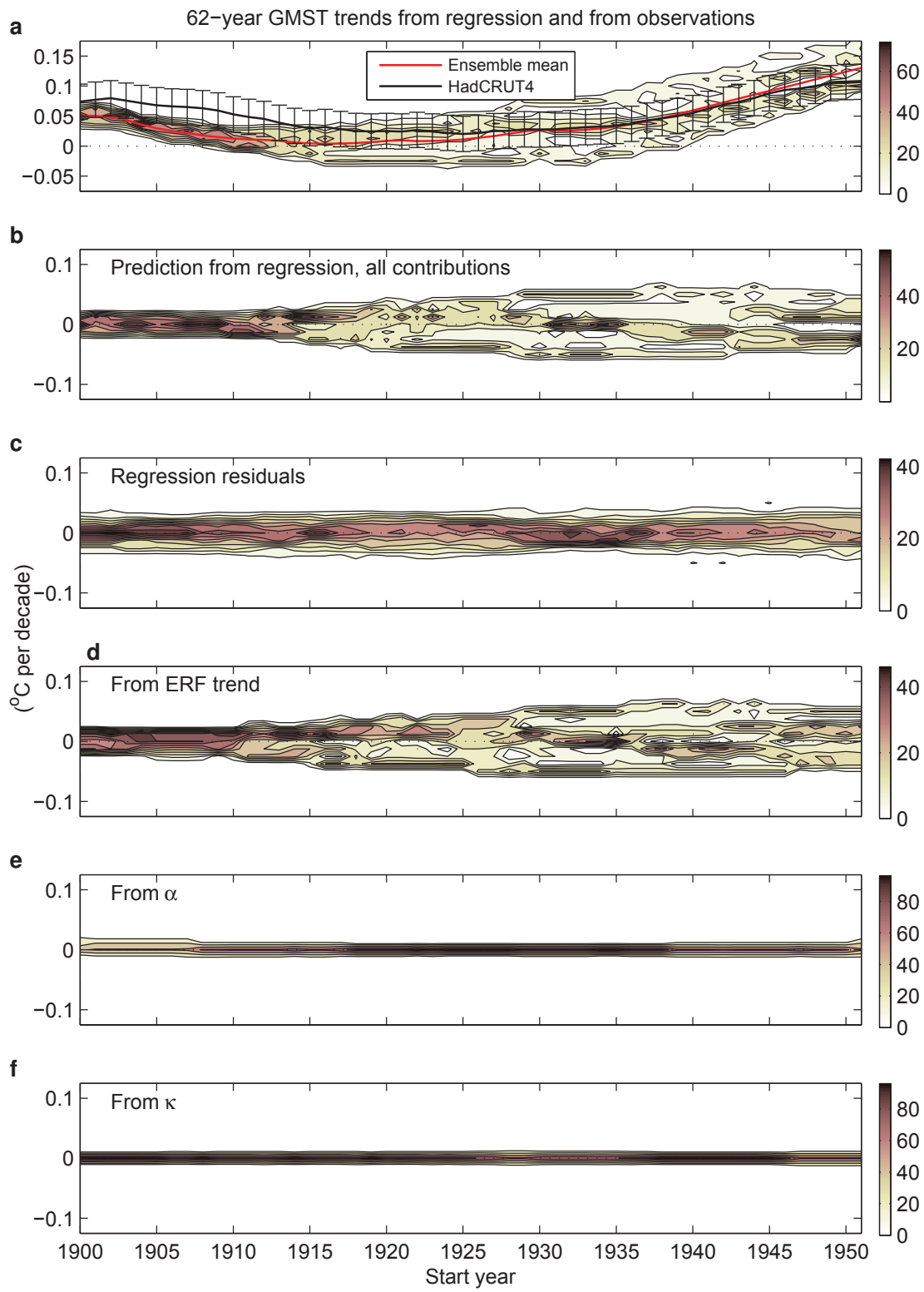


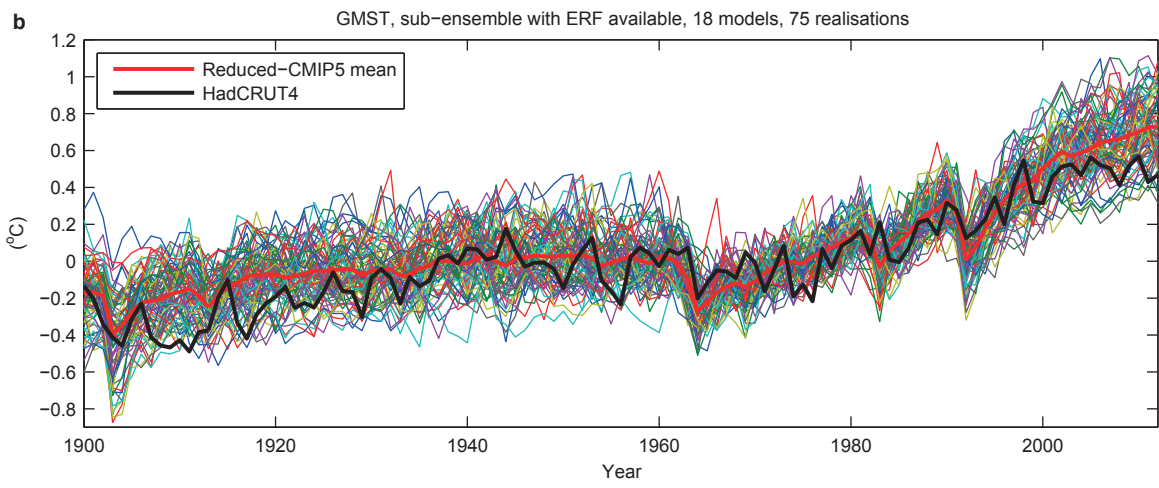
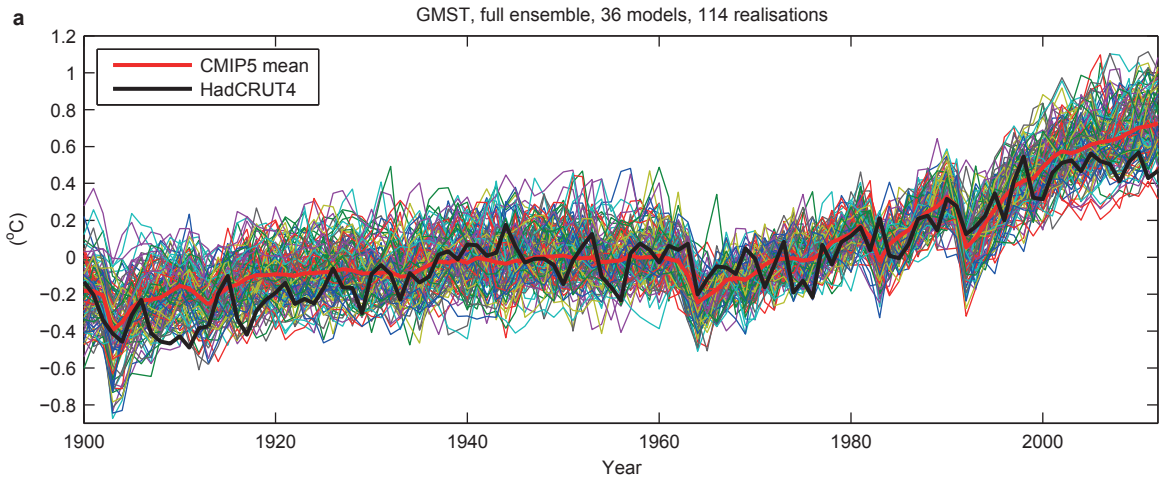
Frequency(rank)

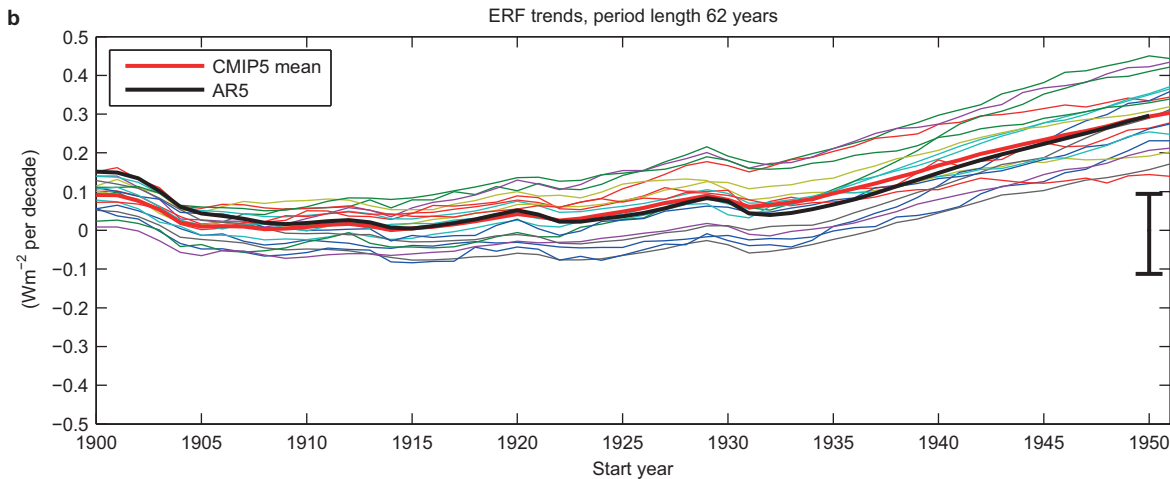
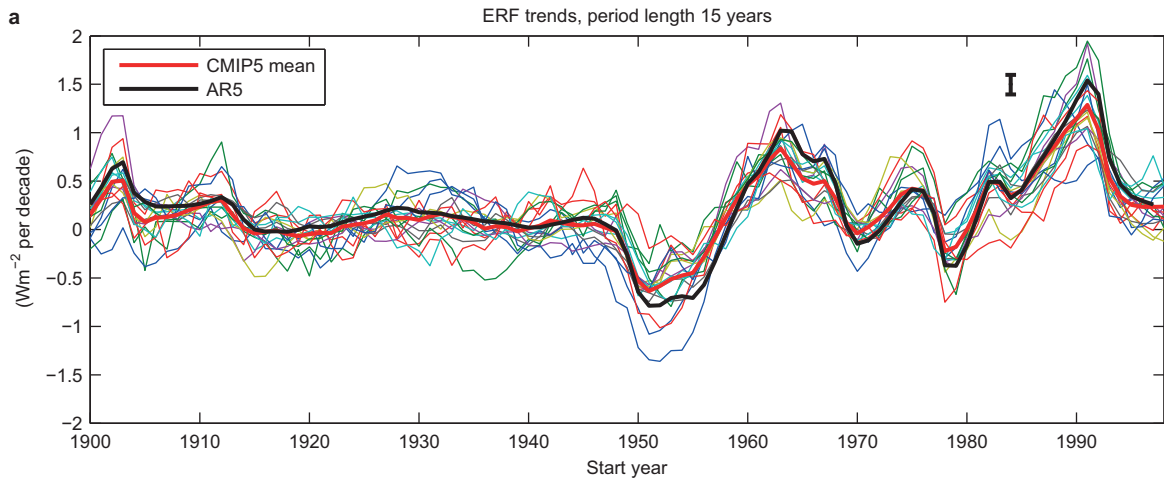


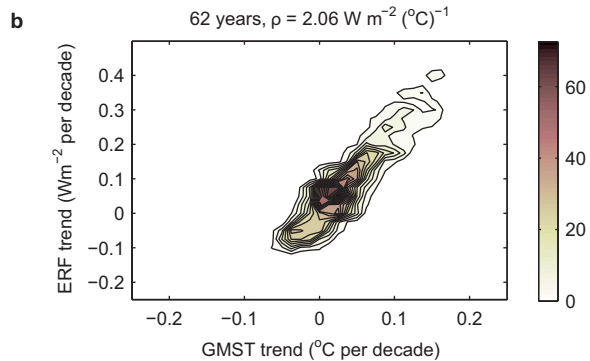
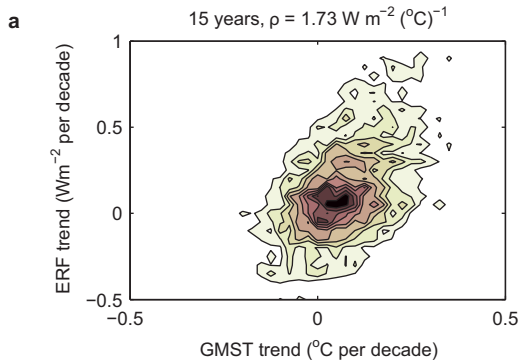
a 15-year GMST trend from regression and from observations



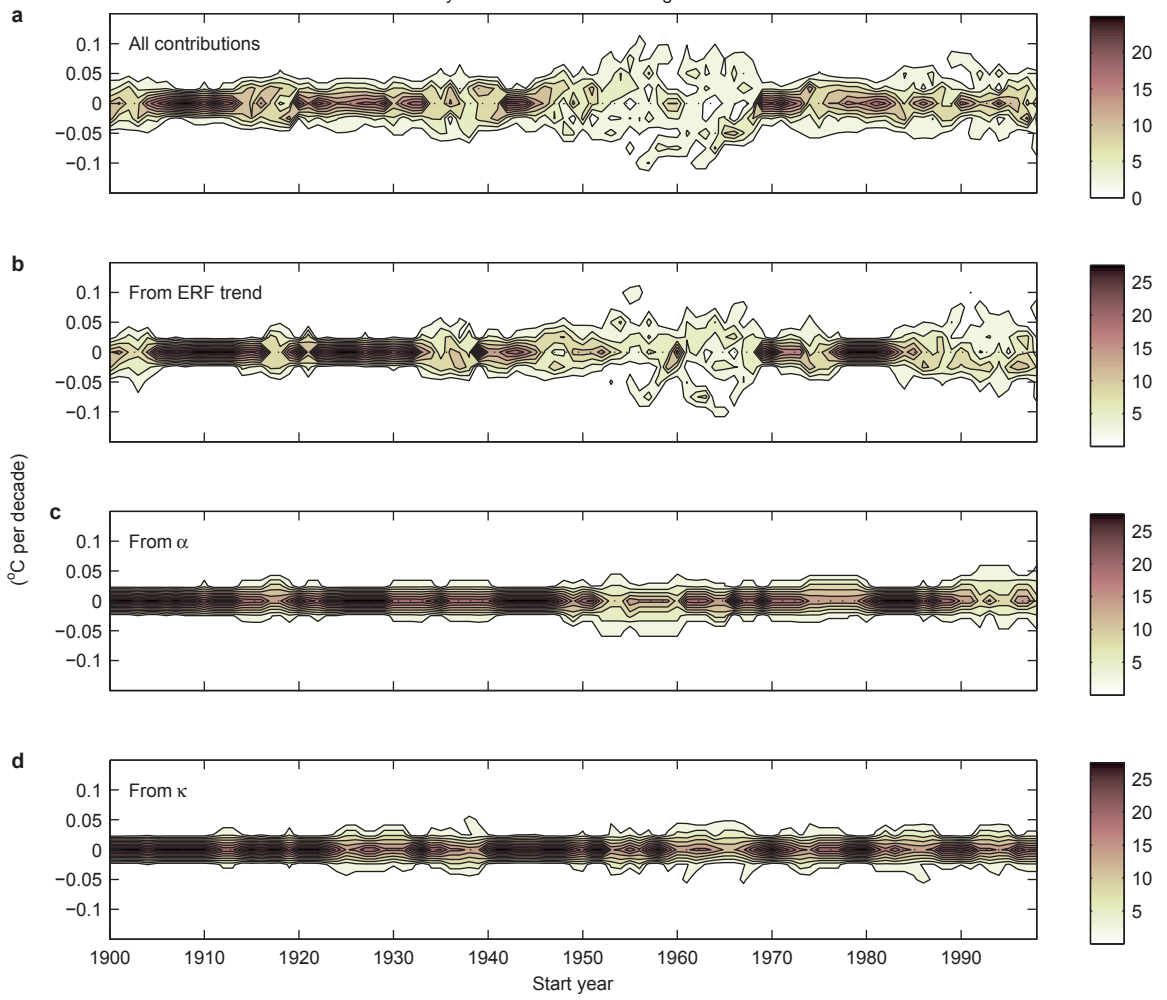








15-year GMST trends from regression



Model name	Number of realisations	Forcing available?
ACCESS1-0	1	Y
ACCESS1-3	1	
bcc-csm1-1	3	Y
bcc-csm1-1-m	3	Y
BNU-ESM	1	
CanESM2	5	Y
CCSM4	6	Y
CESM1-BGC	1	
CESM1-CAM5	3	
CMCC-CM	1	
CMCC-CMS	1	
CNRM-CM5	10	Y
CSIRO-Mk3-6-0	10	Y
FIO-ESM	3	
GFDL-CM3	5	Y
GFDL-ESM2G	1	Y
GFDL-ESM2M	1	Y
GISS-E2-H	5	
GISS-E2-H-CC	1	
GISS-E2-R	6	Y
GISS-E2-R-CC	1	
HadCM3	10	
HadGEM2-AO	1	
HadGEM2-CC	1	
HadGEM2-ES	1	Y
IPSL-CM5A-LR	6	Y
IPSL-CM5A-MR	3	
IPSL-CM5B-LR	1	
MIROC5	5	Y
MIROC-ESM	3	Y
MIROC-ESM-	1	
MPI-ESM-LR	3	Y
MPI-ESM-MR	3	
MRI-CGCM3	3	Y
NorESM1-M	3	